

1-1-2000

# Solid state phase transitions characterized by esr and xas

Juana Vivó Acrivos

San Jose State University, [juana.acrivos@sjsu.edu](mailto:juana.acrivos@sjsu.edu)

Follow this and additional works at: [https://scholarworks.sjsu.edu/chem\\_pub](https://scholarworks.sjsu.edu/chem_pub)

 Part of the [Physical Chemistry Commons](#)

---

## Recommended Citation

Juana Vivó Acrivos. "Solid state phase transitions characterized by esr and xas" *Solid State Sciences* (2000): 807-820. doi:10.1016/S1293-2558(00)01089-X

This Article is brought to you for free and open access by the Chemistry at SJSU ScholarWorks. It has been accepted for inclusion in Faculty Publications, Chemistry by an authorized administrator of SJSU ScholarWorks. For more information, please contact [scholarworks@sjsu.edu](mailto:scholarworks@sjsu.edu).

# Solid State Phase Transitions Characterized by ESR and XAS

Acrivos, Juana Vivó

*San José State University, One Washington Square, San José, CA 95192-0101,*

**To Appear Solid State Science, December, 2000**

## Abstract:

Measurements of the relaxation time,  $\tau$  of electron systems to a disturbance, by two different spectroscopic methods are examined in detail, with the purpose to establish how the presence of fluctuations near a solid state phase transition are made evident in insulators, conductors and superconductors. The absolute temperature and the relaxation time determine the thermodynamic stability of the electronic system near a phase transition by the Uncertainty Principle. At a given temperature  $T$ , Landau and Lifshitz obtain the stability from the lower limit of the uncertainty in entropy in units of the Boltzmann constant,  $\Delta S/k_B \ll 1$  when  $T \tau \gg 3.82$  K ps. Magnetic resonance can measure  $\tau \gg 10^{-10}$  s, when  $\nu = 9$  GHz. X-ray spectroscopy can measure  $\tau \leq 10^{-16}$ s for  $h\nu > 5$  keV. The results extract information about phenomena that occur at the phase transition by following the evolution of spectral features versus  $T$  and crystal orientation. Electron spin resonance identifies the phase transition by the evolution of doublet, triplet and antiferromagnetic resonance, and energy loss. Analysis of the x-ray absorption near an element edge determines one, the relative valence:  $V(\text{Cu in chains}) - V(\text{Cu in planes}) \approx 1$  in  $\text{YBa}_2\text{Cu}_3\text{O}_{7-\delta}$ , two, the appearance of allowed Cu K pre-edge quadrupole transitions at  $T_c$ , three, the enhancement of Ba L<sub>3,2</sub> edge transitions by an order of magnitude, just above  $T_c$ , at a crystal orientation of the c-axis to the x-ray polarization of  $8\pi/18$ , and four, difference x-ray absorption spectra, relative to the transition temperature, identify the bonds as well as the atoms involved in the transition. The figure abstract shows the changes in electron density obtained by temperature difference x-ray absorption near the Y K-edge in  $\text{YBa}_2\text{Cu}_3\text{O}_{7-\delta}$  below  $T_c$ .

## Introduction:

J. M. Honig has devoted a great part of his career to solving solid state chemistry problems using the concepts of physics and of physical chemistry. One important part of his contributions is the study of magnetic phase transitions and their relation to the metal to insulator transition. Spin - spin interactions give rise to the magnetic properties of the electronic system, which may be paramagnetic, antiferromagnetic, superconducting/diamagnetic and/or ferromagnetic on either side of the metal to non-metal transition<sup>1a</sup>. This work uses the concepts developed during the 20<sup>th</sup> century by J. M. Honig<sup>1b</sup> on ferromagnetism and antiferromagnetism, and by N. F. Mott on the metal to non-metal transition<sup>1a</sup> to understand the relaxation time measured by two different spectroscopic techniques, electron spin resonance (esr) and x-ray absorption spectroscopy (XAS) in low dimensional solids (LDS).

The metal to non-metal and the ensuing magnetic phase transition, produced by the onset of spin exchange interactions, are identified by the simultaneous changes in magnetism and metallic behavior. These phenomena have been detected in solids such as  $\text{NiS}_{2-x}\text{Se}_x$ <sup>1b,2</sup>, organic metals, and the superconducting cuprates<sup>3</sup>. The onset of the Mott Transition occurs as the free electron concentration approaches a critical value<sup>1a</sup>:

$$n_{\text{Mott}} = (0.26/a_{\text{H}})^3. \quad (1)$$

$a_{\text{H}} = D a_{\text{bohr}} m_e/m^*_e$  is the hydrogenic radius corrected for the dielectric constant of the medium,  $D$ , and the ratio of the free electron mass to the effective value in the medium,  $m_e/m^*_e$ . The electron concentration is defined by  $a_{\text{H}}^{-3}$  that is two orders of magnitude greater than  $n_{\text{Mott}}$ . This means that the electron-cation and electron-electron spin correlations are very important for electron transport, be it in solid conductors or in dynamic chemical equilibrium to produce new compounds in solution. Since the electrons have an associated spin 1/2, some kind of magnetic order is also introduced at the Mott Transition. The displacement to a superconducting or an antiferromagnetic phase at the Mott Transition is still the subject of study and speculation this

century. Measurements of the system relaxation time, near the transition can be used to ascertain the presence of critical fluctuations that determine the displacement of the equilibrium:

$$\text{Antiferromagnetism}_{\text{extended}} (\uparrow\downarrow) \Leftrightarrow \text{spin pairing fluctuations} \Leftrightarrow \text{Superconductivity}_{\text{dynamic}} (\uparrow\downarrow). \quad (2)$$

Antiferromagnetic (AF) resonance and esr, and XAS are used in this work to interpret the dynamics of the displacement in equilibrium (2).

It is of some importance to determine the degree of thermodynamic stability at a given phase transition. The interplay of charge transfer with the formation of charge density waves (CDW) and/or spin density waves (SDW) leads to fluctuations, that determines whether a superconducting or an antiferromagnetic state is formed at the metal to non-metal transition. It has been shown that quantum critical fluctuations mediate singular interactions between quasi-particles, providing a strong e-e pairing mechanism that leads to a quantum critical point<sup>5</sup>. Pure  $\text{La}_2\text{CuO}_4$  undergoes only an antiferromagnetic phase transition. An incommensurate CDW (ICDW) phase ruins the antiferromagnetic domain order in doped  $\text{La}_{2-x}\text{Sr}_x\text{CuO}_4$  when charge transfer is produced by  $\text{Sr}^{+2}$  substitution in the  $\text{La}^{+3}$  layer and leads to a superconducting state when  $x = 0.05$  to  $0.25$ . Understanding these effects will lead to the discovery of other systems.

#### **Landau-Lifshitz Definition of Thermodynamic Stability**

The Boltzmann probability ( $e^{S/k_B}$ ) of a thermodynamic state is determined by its entropy  $S$  in units of the Boltzmann constant  $k_B$ . The system can be treated thermodynamically<sup>4</sup> in relation (2) as long as its relaxation time  $\tau$  is sufficiently long to produce small fluctuations, i.e., when  $\Delta S/k_B \ll 1$  at a given temperature  $T$ . The Uncertainty Principle:

$$\Delta E \tau \sim T \Delta S \tau \geq h/4\pi, \quad (3)$$

where  $\Delta E$  and  $\Delta S$  are the uncertainty in energy and entropy, and  $h$  is Planck's constant obtains:

$$\Delta S/k_B \geq h/(4\pi \tau k_B T) \sim 3.82 * 10^{-12}/\{\tau(\text{s}) T(\text{K})\}. \quad (4)$$

Then, as long as  $\tau T \gg 4$  ps K, the uncertainty  $\Delta S/k_B$  is small compared to unity, and the system can be treated thermodynamically. Here relation (4) is applied to both antiferromagnetic and superconducting systems<sup>2,3</sup> to understand how the displacement in equilibrium (2) works.

### **Experimental: Magnetic Resonance and XAS Measurement of $\tau$ :**

ESR and XAS are sensitive to changes in the relaxation times  $\tau_{\text{state}}$ , but there are limits to the measurement. At  $\nu = 9$  GHz magnetic resonance can only measure  $\tau > 10^{-10}$  s. When  $h\nu > 5$  keV, XAS can measure  $10^{-16}$  s  $> \tau > 10^{-18}$  s. This leaves a gap in relaxation times not accessible to our measurement, between  $10^{-10}$  s  $> \tau > 10^{-16}$  s which may or may not be important, as described below.

Magnetic resonance measurements on superconductors and antiferromagnetic materials, near a phase transition, using a Bruker 300 EMX system with Oxford 900 cryogenic control are carried out as described elsewhere<sup>3b-d</sup>. Neither esr nor AF resonance from room temperature to  $T_c$  is observed<sup>2</sup> for the superconducting cuprates and  $\text{NiS}_{2-x}\text{Se}_x$ .  $\text{YBa}_2\text{Cu}_3\text{O}_{7-\delta}$  shows a triplet state (T) half field esr absorption (with a forbidden spin  $\mathbf{S}$  transition  $\Delta S = 0$ ) below  $T_c$  (Figure 1a), but  $\text{Nd}(\text{Ba}_{0.95}\text{Nd}_{0.05})_2\text{Cu}_3\text{O}_7$  powder shows doublet (D) esr absorption<sup>3b</sup> with  $^{143,145}\text{Nd}(I = 7/2)$  hfs (Figure 1b). The organic metal  $(\text{BEDTTF})_3\text{Ta}_2\text{F}_{11}$  (BEDT-TTF represents bis-ethylene,dithiolo,tetiathiafulvalene<sup>3a</sup>) shows AF resonance, D and T esr (Figure 2). AF resonance is detected in  $\text{La}_2\text{NiO}_{4.00}$  from room temperature down to where the transition to superconductivity is detected near 21 K<sup>3c</sup>.

The XAS described here measure the Transmittance<sup>6a</sup>  $T = I_1/I_0$  of the solid. We report the Absorbance:

$$A = \text{Log}_{10} (I_0/I_1). \quad (5)$$

The radiation intensity ( $I_i$ ) is measured before and after the sample. A reference compound is placed between ionization chambers  $I_1$  and  $I_2$  to monitor the monochromaticity and stability of the x-ray beam (Figure 3). Measurements, at the Stanford Synchrotron Radiation Laboratory

(SSRL) third generation synchrotron facility, provide x-ray beam monochromaticity and ion chamber stability to allow for the measurement of the Absorbance ( $A_\nu = -T_\nu$ ) of powders and single crystals, at the frequency  $\nu$ . The x-ray energies are determined by the angle  $\Theta$  that an incident x-ray beam makes with two parallel Si crystals in a monochromator; the possibility of higher harmonics is always present and must be addressed in every experiment in order to eliminate measurement uncertainties. When there is a fraction  $x$  of higher harmonics  $n\nu$  ( $n \geq 2$ ) in the beam:

$$I_{0,\nu} = (1 - x) I_0, \quad \sum_n I_{0,n\nu} = x I_0, \quad I_{1,\nu} = (1 - x') I_1, \quad \sum_n I_{1,n\nu} = x' I_1, \quad \text{where } x'/(1 - x') = x 10^{A_\nu}/(1 - x).$$

The measured value  $A \rightarrow A_\nu$  only as  $x \rightarrow 0$ , i.e.,

$$A_\nu - A = \text{Log}_{10}((1 - x)/(1 - x')) = \text{Log}_{10}(1 + x(10^{A_\nu} - 1)) \rightarrow x(10^{A_\nu} - 1)/\text{Ln}10 \geq 0, \quad \text{as } x \rightarrow 0. \quad (5')$$

Monochromaticity of the beam is achieved by detuning the second Si crystal in the monochromator from the exact diffraction angle by  $\Delta\Theta$  with a piezoelectric device (Figure 3). Negligible harmonic content is usually obtained by 80% detuning of  $I_0$ . The higher harmonics  $n\nu$  are eliminated because they are narrower than the fundamental diffraction, which is then shifted by the amount  $\Delta E = E \cot \Theta \Delta\Theta$ . The monochromaticity of the beam is determined by the limit of  $A/A_\nu = 1$  which produces near the Cu –K edge a 4 eV shift as  $x \rightarrow 0$  with a 111 Si cut crystal (Figure 5 of ref. 6b). Latimer et al.<sup>6c</sup> have confirmed this by intensity measurements of the fundamental and harmonics; 80 % detuning does indeed produce a pure beam. Throughout an experiment the stability of  $A_\nu$  and  $E_0$  for the reference compound is used to determine the limits of accuracy. The rejection of the higher harmonics depends on the edge being measured and must be done for every experiment. The raw data for the sample versus temperature  $T$  is only analyzed after the reference at room temperature shows the desired stability obtained with an  $I_0$  detuning of 80%. The Absorbance versus temperature (Figures 4 to 7) is obtained from the raw data as described in the literature<sup>11</sup>. The temperature is monitored with an Oxford 9000 cryogenic system and recorded digitally with Oxford ObjectBench PC software. Typical

measurements are carried out in complete temperature cycles. The samples were prepared at different laboratories (Parkin at IBM, ref. 3d, Lin at the IRC for Superconductivity, ref. 7, and Honig's Group at Purdue, ref. 1b and 3b). The temperature dependence of the cuprate superconductors XAS (Figures 4 to 6) and antiferromagnetic insulators (Figure 7) are used to ascertain the differences in the respective phase transitions.

### **Discussion: $\tau$ from ESR/XAS**

**A.** The magnetic properties measured at 9 GHz obtain the relaxation time to within a lower limit of to  $10^{-10}$  s.

1. The lower limit of  $\Delta S/k_B$  versus temperature for  $(BEDT-TTF)_3Ta_2F_{11}$  (Figure 8) shows the effects of spin-spin interactions. Three regions are identified by the lower limits of the uncertainty in  $\Delta S/k_B$ :

1.1 Doublet (D) and AF domains coexist for  $T > 10^2$  K and the lower limit of  $\Delta S(D, AF)/k_B$  (Figure 8) increases as T decreases indicating the approach to a phase transition; the D esr line shape changes from Lorentzian to Gaussian near 150 K and  $\tau_{AF} < 10^{-10}$  s below 85 K.

1.2 When  $10^2 \geq T > 10^1$  K, the D and triplet (T) states coexist and the uncertainty in entropy  $\Delta S(D, T)/k_B$  increases as T decreases (Figure 8).

1.3 As  $T \rightarrow T_c \leq 10^1$  K,  $\Delta S(D)/k_B$  increases by two orders of magnitude whereas the lower limit of  $\Delta S(T)/k_B$  decreases by the same amount at  $T_c$ . Saturation measurements indicate that near  $T_c$  the triplet states have a relaxation time twice as long as the doublet states and that only the triplet esr absorption has Dysonian shape<sup>6d</sup>. A change in the spin-lattice relaxation time, given by the phenomenological Gorter relation<sup>6d</sup>:

$$\tau_1(T) = C_H(T)/\alpha_H(T)$$

is produced by the changes in the thermal heat capacity  $C_H(T)$  and in the thermal transport coefficient  $\alpha_H(T)$  at constant field H:

$$\Delta(\tau_1)/\tau_1 = \Delta(C_H)/C_H - \Delta(\alpha_H)/\alpha_H.$$

An increase in  $C_H(T)$  near  $T_c$  is reflected in  $\tau_1(T)$ , which suggests that the triplet state is in thermal contact with the superconducting Bose pairs. An increase in the thermal transport coefficient, which is expected to occur below  $T_c$  decreases  $\tau_1$  back to the original value<sup>3e</sup> (since the maximum in  $\alpha_H$  for  $YBa_2Cu_3O_{7-\delta}$  occurs  $\sim 30$  K below  $T_c$ , identified by the maximum in  $C_H$ <sup>10f</sup>). As  $T \rightarrow 4$  K both doublet and triplet states are stable with a lower entropy uncertainty limit  $\Delta S/k_B \geq 10^{-5.6}$ , but the D state esr line shape indicates that it does not arise from a metallic phase.

2. The superconducting cuprates have different esr absorption than the organic metals:

2.1 Only triplet esr absorption (with a forbidden spin transition  $\Delta S = 0$ ) is observed below  $T_c$ , at half field, for  $YBa_2Cu_3O_{7-\delta}$ ; the state is stable with a lower entropy uncertainty limit  $\Delta S/k_B \geq 10^{-5.8}$ . In both the superconducting cuprate and the organic metal single crystals, the Dysonian shaped  $\Gamma$  esr absorption must arise from the normal metal region induced by the finite field of 156 mT and this is different whether the sample is cooled through  $T_c$  in a magnetic field or not (Figure 1a). Magnetic oscillations are observed in field cooled samples as  $H$  increases.

2.2 Doublet state esr (with an allowed spin transition  $\Delta S = 1$ ) is observed in  $Nd(Ba_{0.95}Nd_{0.05})_2Cu_3O_7$  at room temperature<sup>3a,b</sup>. Two centers (c1 and c2 in Figure 1b with  $g \approx 2$ ) show different relaxation times  $\tau_1(D_{c2}) \approx 10^2 \tau_1(D_{c1})$  at room temperature. The nuclear hfs indicates that the c2 centers (Figure 1b) are associated with Nd paramagnetic centers. Both the c1, c2 esr disappears at  $T_c$  due to the Meissner effect<sup>3a,b</sup>.

3. AF resonance spectra from pure  $La_2NiO_{4.00}$ <sup>3c</sup> measure a relaxation time that gives the lower entropy uncertainty limit for the antiferromagnetic state  $\Delta S(AF)/k_B$  versus  $T$  (Figure 9). Near  $T_c \approx 21$  K the lower limit for the entropy of fluctuations is  $\Delta S(AF)/k_B \geq 10^{-4}$ . Superconducting and antiferromagnetic states are found to coexist in  $La_2NiO_{4.00}$  in the range  $21 > T > 4$  K<sup>3b</sup>. Inability to saturate these signals rules out any inhomogeneous broadening.



**B.** The XAS measurements are made above  $\nu \sim 10^{15} \text{ s}^{-1}$ . The x-ray absorption near the edge spectra (XANES) provide information on the transitions from the core to discrete states near the edge. The x-ray absorption fine structure (XAFS) near a phase transition measure any changes in bond distance and/or Debye-Waller factor<sup>2,8-12</sup>. The XAFS are less than ten percent of the total Absorbance. The atomic (AT) XAS makes up the rest, and is also important in the study of phase transitions. The AT-XAS provide information on: the density of final states, the relaxation times of the final states<sup>9a</sup>, the presence of fluctuations in the atomic potential, how these affect the relaxation time, and how the changes in the electron density, near the absorber  $A$ , determine the so called atomic (AT) XAFS<sup>9b-e</sup>. The latter are observed in heavy elements at distances less than an angstrom. The excitation of core electron to states in a continuum of high kinetic energy states, probe the atomic potential for the absorber  $A$ . The angular dependence of the x-ray absorption cross section<sup>9f</sup> for a particle of mass, charge and spin  $s$  gyromagnetic ratio ( $m_e, q, g$ ) in a potential  $V(r)$  and electromagnetic field ( $\Phi, \mathbf{A}$ ), of frequency  $\omega = 2\pi\nu$ , crossing the unit area, normal to the propagation direction, at the rate  $I(\omega) = 2 \epsilon_0 c |\mathbf{A}_0|^2 \omega^2$  is obtained from:

$$H = H_0 + [i q \hbar/2\pi m_e \mathbf{A} \cdot \nabla + \hbar c] + q^2/2m_e A^2 + q \Phi - (g q/2m_e) \mathbf{s} \cdot \mathbf{B}, \quad (6)$$

where  $H_0 = -(\hbar/2\pi)^2 \nabla^2 + V(r)$ ,  $\mathbf{A}(\mathbf{r}, t) = \mathbf{A}_0 \boldsymbol{\epsilon} e^{i(\mathbf{k} \cdot \mathbf{r} - \omega t)} + \text{hc}$ ,  $\epsilon_0$  is the permittivity of vacuum,  $c$  is the velocity of light,  $\boldsymbol{\epsilon}$  is the unit polarization vector,  $\mathbf{k}$  the x-ray wave vector and  $2^{1/2} \mathbf{A}_0$  the vector potential amplitude. The transition probability for a perturbation  $W(t) = W e^{-i\omega t} + \text{hc}$ , per unit time in first order,  $w = 4\pi^2/\hbar \sum_f |\langle f|W|i \rangle|^2 \delta(E_f - E_i - \hbar\nu)$ , for a plane wave ( $\mathbf{B} = \nabla \times \mathbf{A}$ ) is:

$$w = (4\pi^2 q^2 / \hbar m_e^2) |\mathbf{A}_0|^2 \sum_f |\langle f| e^{i(\mathbf{k} \cdot \mathbf{r} - \omega t)} \{ \hat{\boldsymbol{\epsilon}} \cdot \nabla / 2\pi - (g/2) \mathbf{s} \cdot [\nabla \times \mathbf{k} \times \hat{\boldsymbol{\epsilon}}] |i \rangle|^2 \delta(E_f - E_i - \hbar\nu),$$

and the absorption cross section in the absence of magnetic interactions is<sup>9f</sup>:

$$\sigma(\omega) = (w \hbar\nu) / I(\omega) = 2\pi \alpha \hbar w \sum_{g,i,f} \{ |\langle f|\hat{\boldsymbol{\epsilon}} \cdot \mathbf{r}|i \rangle|^2 + 0.25 |\langle f|\hat{\boldsymbol{\epsilon}} \cdot \mathbf{k} \cdot \mathbf{r}|i \rangle|^2 + \dots \} \delta(E_f - E_i - \hbar\nu). \quad (6.1)$$

The atomic absorption cross section  $K_A$  versus energy,  $E = h\nu$ , in the neighborhood of an x-ray edge ( $E_0 = h\nu_0$ ) for the absorber  $A$ , is given by the sum of Lorentzian curves<sup>9a</sup> (Appendix I):

$$K_A(\tau, (\nu - \nu_0)) = \sum_{AE} a_A / [1 + (2\pi \tau)^2 (\nu_{AE} - \nu)^2] \rightarrow C_A \{ \pi/2 + \text{atan}(2\pi \tau (\nu - \nu_0)) \}, \quad (6.2)$$

where  $a_A$  and  $C_A$  are constants determined by the material and  $h\nu_{AE}$  is the excitation energy. The atomic potential determines the states' lifetime. In the absence of fluctuations:

$$1/\tau = 1/\tau_{if} = (1/\tau_{\text{initial states}} + 1/\tau_{\text{final states}})/2.$$

For energies below an edge (near 5 to 13 keV) the natural relaxation times are determined from the magnitude of the half line widths (0.5 to 1 eV) to be  $\tau_{if} \geq 10^{-16}$  s. The photoelectron emitted by  $A$  travels to  $B$  at a bond distance  $R_{AB} \sim 3 \text{ \AA}$  and back in less than  $10^{-17}$  s. In the absence of fluctuations the measured relaxation time is  $\tau = \tau_{if}$ . In the presence of fluctuations in the potential, which limits the lifetime of the final state,

$$1/\tau = 1/\tau_{if} + 1/\tau_{\text{fluctuations}}.$$

Thus, the XAS are ideally suited to measure changes in the relaxation times of the order  $10^{-16}$  to  $10^{-17}$  s near a phase transition. At room temperature, the XANES line widths give the natural lifetime of the final states of  $10^{-16}$  s<sup>11</sup>. Any decrease in  $\tau$  below  $10^{-16}$  s can be detected by its effect on the atomic absorption coefficient  $K_A$ . We have developed a method that measures x-ray temperature difference absorption spectra (XTDAS)<sup>2a,b</sup> (Figures 4 to 7). Appendix I lists the textbook parameters for x-ray Absorbance of a metal<sup>9,11</sup>. The Absorbance,  $A_{vA}(T_0)$ , at or above the phase transition temperature  $T_0$ , is used as a reference spectrum, and the difference spectrum is defined as:

$$\text{XTDAS}(T) = \{A_{vA}(T) - A_{vA}(T_0)\} \text{ or } \text{XTDAS} * k^3. \quad (7)$$

The data in Figures 4 to 7 are used to differentiate between several types of phenomena at the phase transition,  $A_{vA}$  and the photoelectron wave-vector  $k$  are defined in Appendix I. When there are neither structural nor electronic changes near  $T_0$  the XTDAS vanish. A non-zero difference identifies the phenomena that occur near the phase transition:

1. The XANES depend on the relaxation time of the final states in  $\text{YBa}_2\text{Cu}_3\text{O}_{7-\delta}$  single crystal and powders.s

1.1 In a  $\text{YBa}_2\text{Cu}_3\text{O}_{7-\delta}$  single crystal (CT) with Absorbance thickness  $d_c \sim 44 \mu\text{m}$  (determined at the Cu K, Ba L3,2 and Y K- edges in Figures 4-6), dipolar edge transitions, Cu  $1s \leftrightarrow n p_i$  states are observed (Figures 4d-f) separated by  $\sim 7 \text{ eV}$ . These are identified by the orientation dependence versus  $\theta = c^{\wedge}\epsilon_{\text{x-rays}}$  (Figures 4d-f). The data is manipulated; first the absorbance is normalized to zero XAFS amplitude,  $\mu_A = A/A_{\text{XAFS},0}$ , then the XANES intensity is obtained,  $\mu_{\text{AE}} = \mu_A - \{1/2 + \sum_i(x_i \text{atan}(m(E - E_{0i}))/\pi)\}$  when  $m = 2 \pi \tau/\hbar \sim 0.3/\text{eV}$  ( $\tau = 2.2 \text{ E-}16 \text{ s}$ ) and the mole fractions are  $x_i = 1/3, 2/3$  for Cu in the CuO chains and in the  $\text{CuO}_2$  planes respectively.  $E_{0i=\text{chains-}} E_{0i=\text{planes}} = 6 \text{ eV}$  gives a good fit to the spectra averaged over  $T = 49$  to  $100 \text{ K}$  which suggests a valence difference  $V(\text{Cu in chains}) - V(\text{Cu in planes}) \approx 1$ .over the entire  $T$  interval. The dipolar contribution,  $\mu_{\text{CuEn}}(\theta) = \mu_{\text{CuE}}(\theta)/\cos(\theta) \sim \text{constant}$ , indicates the final states have  $np_{x,y}$  symmetry. Although the sample geometry prevents obtaining data for  $\theta < \pi/4$ , a  $p_z$  component for the final states is identified from  $(\mu_{\text{CuEn}}(\pi/4) - \mu_{\text{CuEn}}(\pi/2))/\sin(\pi/4)$ . Transitions which are two orders of magnitude lower in amplitude than those above appear only when  $K_{\text{Cu}}$  decreases for high photoelectron kinetic energy, near  $T_c$  (Figures 4a-c). They are broad. Line widths of the order of  $\sim 10 \text{ eV}$  obtain  $\tau \sim 6.6 \cdot 10^{-17} \text{ s}$ , which suggests that the final states are associated with nd conduction band states that become vacant only near  $T_c$

1.2 At the Ba L3,2 edges:  $2p_{3/2,1/2} \leftrightarrow nd$  XANES and XAFS are sharp (with less than 3 eV line widths) for all  $T$  when  $\theta = \pi/2$ . Rotation from  $\theta = \pi/2$  to  $\theta = 8\pi/18$ , produces a signal enhancement which increases as the temperature is lowered below  $120 \text{ K}$  (Figure 5a). The enhancement is over an order of magnitude (Figure 5b-e) and an interference pattern is observed with a period of  $0.67 \text{ eV}$ . This is the first observation of such phenomena. It can be qualitatively explained by the propagation of electromagnetic radiation into the crystal by x-ray diffraction from planes containing the Ba atoms coupled by a surface plasmon (when this appears at a given

temperature  $T < 121$  K) in a way which is similar to surface enhanced Raman scattering. Near  $\lambda = 2.36$  Å (Ba-L3 edge) and  $2.20$  Å (Ba-L2 edge), at  $\theta = 8\pi/18$ , there are Ba diffraction planes<sup>10i,j</sup>. The scattering vector for an (hkl) plane is given by the Bragg condition,  $S_{hkl} = 2 \sin(\theta_{hkl})/\lambda$ ; the diffracted wave length in the  $i^{\text{th}}$  layer  $\lambda_i = E_i/hc$  is determined by the index of refraction:  $\lambda_i/\lambda_{i+1} = n_{i+1}/n_i$ ; The expression for  $n = 1 - \delta - i\beta^{10h}$  allows to estimate  $\delta/\text{layer} \sim 7.7 \cdot 10^{-6}$  for planes containing the Ba atom. If the interference period  $dE = 0.67$  eV is produced by an energy shift, on flux enhancement by diffraction, this must occur over 17 ~layers of sample or  $\sim 21$  nm of sample which is smaller than the sample thickness  $d_c$ . This new phenomenon must be associated with the vibrational modes in the lattice that involve the Ba atoms<sup>10b,c</sup>. Recent work<sup>10b</sup> shows that the Raman vibrational modes involving the Ba atoms and the O3A and O3B atoms soften above 100 K in the related compound  $\text{YBa}_2\text{Cu}_4\text{O}_8$ <sup>10b</sup>. The bonds responsible for the enhancement are described below by the analysis of the XTDAS in the XAFS region. The phenomenon is not observed at Cu-K edge of CT and neither did Howland et al., observe it at the Zn K-edge when they studied the anomalous Bragg enhancement of diffraction in  $\text{YBa}_2\text{Cu}_{3-x}\text{Zn}_x\text{O}_{7-\delta}$ <sup>10a</sup>. Weak interference fringes are observed at  $E_{0,Y \text{ K-edge}} \sim 3 E_{0,Ba \text{ L2-edge}}$ , the CT Y K-edge, at the same orientation, as described below (Figure 6b).

1.3 The CT crystal Y K-edge XANES (Figure 6) have a similar orientation dependence as those observed near the Cu K-edge. Interference structure of 1.3 eV is observed at  $\theta = 35\pi/72$ . The XTDAS show angular dependence (Figure 6c-f). The lack of measurable enhancement (Figure 6a, b) suggests that only a small fraction of the Y atoms are responsible for the interference effect; these may occur as impurities in the BaO layer.

2 Changes in the metal density of states  $N(E)$  (Appendix I) near the Fermi energy,  $E_F$ , or in the atomic relaxation time  $\tau_{if}$  in relation (6.2) will change  $K_A$ . The plots of the Richtmyer relation for the absorption coefficient,  $K_A(m = 2\pi \tau/h, (E-E_0))$  versus  $(E-E_0)$  have a positive slope,  $dK_A/d(E-E_0)$  versus  $E-E_0$  when  $\tau$  is independent of  $E-E_0$ , which is not found experimentally. The

data (Figures 4 to 7) indicate that  $\tau$  is determined at the absorption edge by the lifetime of the discrete final states, and that it decreases as the kinetic energy of the final states increases, indicating a dependence on the presence of fluctuations in the local potential  $V(r)$  in relation (6), near a phase transition. The calculated slope,  $(K_A - 1)/(E - E_0)$  versus  $m$  and  $E - E_0$  and the experimental spectrum are used to obtain the relaxation time  $\tau$ . Since the relaxation time increases to the normal value at temperatures below  $T_c$ , any changes of  $E_F$  in the superconducting state do not appear to affect  $K_A$ .

3 Near the Ba-L3 edge, the XTDAS and weighted  $k^3$ XTDAS show oscillations in the XAFS region for a  $YBa_2Cu_3O_{7-\delta}$  single crystal, and for powder  $Nd(Ba_{0.95}Nd_{0.05})_2Cu_3O_{7-\delta}$  ) which are analyzed for causes:

3.1 Atomic (AT) XAFS observed in the Fourier Transform at  $(R_{\text{electron density}} + \Delta)$  of less than an Ångstrom are hard to interpret in condensed phases, because of the scattering from nearby atoms; these features can only be isolated in the x-ray absorption spectra of gases<sup>9b,c</sup>. AT-XAFS have been identified in the  $Rb^+$  vapor power spectrum<sup>9c</sup>. However, if in a phase transition the only change that occurs is in the electron density near a given site, it may be detected for a heavy atom absorber (Ba, Y). Then short wave length oscillations are observed in the XTDAS versus the photoelectron wave vector  $k$  (Figures 5f, g and 6c-e). The oscillations repeating at  $\Delta k \simeq 4.5 \text{ \AA}^{-1}$  (Figure 5g) do not correspond to a bond change but to a change in electron density near the Ba atom near  $T_c$  for  $Nd(Ba_{0.95}Nd_{0.05})_2Cu_3O_7$ . The advantage of XTDAS here is that the XAFS contributions from all the other bonds were subtracted out, allowing to identify the bonds and electron density changes at the phase transition.

3.2 The weighted  $k^3$ XTDAS for CT, at the Ba L3-3d edge (Figure 5f) between  $T$  and  $T_c \sim 60 \pm 2 \text{ K}$  (second superconducting phase transition, identified by the decrease in AT-XAS at high photoelectron  $k$ , near the Cu K-edge in Figure 4d) shows an oscillation of approximately the same wavelength as for the powder but an order of magnitude more intense. This suggests that the

effect is orientation dependent. The weighted  $k^3$ XTDAS between any two temperatures below  $T_c$  vanish (insert Figure 5f).

4. The anomalous Bragg case for CT diffraction near the L2,3 edges, also affects the XAFS intensity (Figure 5c). If an  $A$ - $B$  bond Debye-Waller factor ( $\sigma_{AB}(T)$ ) is the only change, the XTDAS can be used to identify the bond involved. Then in relation (I.1) Appendix I:

$$k^3 * \text{XTDAS} = k^2 (\exp(-2k^2\sigma_{AB}^2(T)) - \exp(-2k^2\sigma_{AB}^2(T_0)))$$

$$S_A(k) F_B(\pi,k) N_{AB} \sin(\phi_B(T) + 2 k R_{AB}(T))/(R_{AB}(T)^2). \quad (7')$$

The  $A$ - $B$  bond vibrational modes cause  $\sigma_{AB}^2(T)$  to decrease discontinuously at a transition temperature, the XTDAS cancel all the other bond contributions, leaving only the sharp sinusoidal oscillations associated with  $\sigma_{AB}^2(T_0)$ . The oscillations in XTDAS (Figures 5c for CT and 7 for the powder  $\text{NiS}_{2-x}\text{Se}_x$ ) versus  $k$ , are explained by relation (7') and used to identify bonds involved in the respective transitions:

4.1 The sharp XTDAS for CT:  $\text{YBa}_2\text{Cu}_3\text{O}_{7-\delta}$  single crystal near the Ba-L3 edge, that are enhanced below 100 K (Figure 5c) identify the bonds involved as Ba-O3A/O3B. This is in agreement with the Raman studies of Watanabe et al.<sup>10b</sup> where the Ba and the O3-O2 modes were found to soften below 130 K in  $\text{YBa}_2\text{Cu}_4\text{O}_8$ . Below 100 K the weighted  $k^3$ XTDAS between any two temperatures  $92 \text{ K} > T_1, T_2 > 63 \text{ K}$  vanish (insert Figure 5f). However the weighted  $k^3$ XTDAS between  $T_1 = 63 \pm 2 \text{ K}$  and  $T_2 = 56 \pm 2 \text{ K}$  (Figure 5f) indicate the presence of a short wave length oscillation similar to that observed near the same temperature in  $\text{Nd}(\text{Ba}_{0.95}\text{Nd}_{0.05})_2\text{Cu}_3\text{O}_{7-\delta}$  (Figure 5g) caused by changes in the AT-XAS by the electron density change near the Ba atom at  $T_c$ .

4.2 The angular dependence of the CT XTDAS near the Y K-edge, relative to a temperature well above  $T_c$ , produce AT-XAFS (Figures 6b-e) which indicate that below  $T_c$ , the electron density changes asymmetrically near the Y atom, at the presumed unit cell center of inversion.

4.3 The sharp oscillations observed for  $\text{NiS}_{2-x}\text{Se}_x$  (Figure 7) correspond to the Se-Ni bond,  $R_{\text{Se-Ni}} = 2.3 \text{ \AA}$ . The advantage of XTDAS in the study of phase transitions in complicated structures is that only the bond responsible for the transition is selected. When the other bonds also change ( $T \geq 37 \text{ K}$ ) the oscillations in the XTDAS are washed out by interference<sup>2b</sup>.

5 If only the mean free path  $\lambda_{AB}$  of the photoelectron changes and  $R_{AB}/\lambda_{AB} \ll 1$  the XTDAS plotted versus  $1/k$  must vary as the difference in inverse mean paths ( $1/\lambda_{AB}(T_0) - 1/\lambda_{AB}(T)$ ); the effect is expected to be smaller than the  $K_A$  contribution.

**C:** All of the effects described above may be present near a phase transition. A summary of the observations offers a comparison between AF and superconducting transitions:

- Cu-K edge XAS (Figure 4) indicate that there is a decrease in  $\tau_{\text{XAS}}(\text{YBa}_2\text{Cu}_3\text{O}_{7-d})$  from  $\tau_{\text{if}} \geq 10^{-16} \text{ s}$  when  $T \neq T_c$  to  $\tau_{\text{if}} \leq 10^{-17} \text{ s}$  near  $T_c$ . The XANES suggest that Absorbance should be observed near  $h\nu = 10^2 \text{ eV}$ , at  $T \neq T_c$  with 10 eV line widths.

- The calculated atomic absorption coefficient for AT-XAS,  $K_A(m, E - E_0)$  and its slope versus  $m = 2\pi\tau/h$  are used to ascertain the limits of  $\tau$  using relation (6.2):

$$\begin{aligned} m(T)/m(T_c) &= \tau(T)/\tau(T_c) = \\ & (1/10^{-16} \text{ s} + 1/\tau_{\text{fluctuations}}(T_c)) / (1/10^{-16} \text{ s} + \\ & 1/\tau_{\text{fluctuations}}(T)) \rightarrow \tau(T)/\tau_{\text{fluctuations}}(T_c). \end{aligned}$$

or,  $\tau(T_c) < 1/2 \tau(T \neq T_c) \approx 10^{-17} \text{ s}$  (Figure 4a). The lower limit in the entropy uncertainty  $\Delta S(T_c)/k_B \gg 1$  indicates the presence of a quantum critical point in cuprate superconductors.

- ESR data indicate the presence of strong critical magnetic fluctuations, as  $\mathbf{H}$  increases, below  $T_c$  for the single crystals  $\text{YBa}_2\text{Cu}_3\text{O}_{7-\delta}$  and the organic metal, and for the powders  $\text{Nd}(\text{Ba}_{0.95}\text{Nd}_{0.05})_2\text{Cu}_3\text{O}_7$  and  $\text{La}_2\text{NiO}_{4.00}$ .

- Triplet state half field esr with Dysonian line shapes are observed below  $T_c$  in single crystals.

- A change in the electron density near the Ba and Y atoms has been observed in superconducting cuprates (both powder and crystalline) at a nominal distance of less than an Å near  $T_c$ ; this is orientation dependent. Large errors in the bond distances Ba-M near  $T_c$ <sup>2d</sup> are introduced if the AT-XAFS are not taken into account.
- The XTDAS below 100 K near the Ba-L<sub>3</sub> edge (Figure 5c) indicate that the Ba-O3A/B bonds are involved in a mode softening transition, similar to that observed by Raman measurements in YBa<sub>2</sub>Cu<sub>4</sub>O<sub>8</sub><sup>10b</sup>.
- Enhanced Absorbance together with the observed interference fringes of period  $dE$ , suggest that the electromagnetic flux is enhanced by the propagation of radiation by the anomalous Bragg diffraction, near the Ba-L<sub>3,2</sub> edges in CT YBa<sub>2</sub>Cu<sub>3</sub>O<sub>7- $\delta$</sub>  single crystal. Shifts in the wavelength produce interference that is in resonance with a surface vibrational mode (plasmon) of energy  $dE$ . This appears just above  $T_c$ . This type of enhancement has not been observed at the Cu or the Y-K edges for the same crystal orientation.
- The relaxation time limits obtained from the AT-XAS slope indicate that  $\tau(\text{NiS}_{2-x}\text{Se}_x, x = 0.47 \text{ and } 0.6 \text{ near } 75 \text{ to } 80 \text{ K}) \leq 10^{-17} \text{ s}$ , and increases to  $\tau(6 \text{ to } 7 \text{ K}) \geq 10^{-16} \text{ s}$ . The XTDAS oscillations (Figure 7) indicate that the Ni-Se bond is involved in the transition near 6 to 7 K<sup>15</sup>, which causes the bond Debye-Waller factor to decrease discontinuously below this temperature, and that all the other bonds remain unchanged from  $T = 11 \text{ to } 27 \text{ K}$ . The XTDAS (Figure 7) subtracts their contributions to the total Absorbance, leaving only the sinusoidal oscillation associated with the Ni-Se bond, at  $T_0$ . At 37 K structural changes occur, as indicated by the change in the S-Se bond<sup>2b,e</sup> which is associated with disappearance of the structure in XTDAS versus  $\mathbf{k}$  above 37 K because all the XAFS interfere destructively.

### **Conclusions:**



A decrease in the relaxation time  $\tau$  indicates an increase in the lower limit of the entropy uncertainty for the state. However,  $\Delta S(T_c)/k_B \gg 1$  in cuprates indicates that a quantum critical point<sup>5</sup> is responsible for the transition to superconductivity.

#### **Acknowledgments:**

Work supported by NSF-DMR Grant 9612873 and NSF-INT Grant 9312176 between SJSU and the IRC for Superconductivity, Cambridge University for JVA at SJSU. DOE support at SSRL is acknowledged through proposal 2425M. This work could not have been done without the mentors (ref. 1) or the students and colleagues at the IRC (ref. 2,3,7).

## References

1. (a) N. F. Mott, "*Metal to Insulator Transition*", Taylor and Francis, 1974, 1990; (b) J.M. Honig and J. Spalek, *Chem. Mater.*, **10**, 2810 (1998)
2. (a) L. Nguyen, et al., Am. Phy. Soc. March Meeting, *Bull Am Phys. Soc.*, **43**, 345 (1998); (b) T. Norman et al., Am. Phy. Soc. March Meeting, *Bull Am Phys. Soc.*, **43**, 871 (1998); (c) T. Norman, L. Nguyen, A. T. Nguyen, C. M. Burch, T. H. Vu, Q. van Le, J. V. Acrivos, "*Stanford Synchrotron Radiation Laboratory Activity Report*" 2375M, (1997); (d) L. Nguyen, "*MS Thesis*", SJSU (1999); (e) T. Norman, "*M.S. Thesis*", SJSU (1999)
3. (a) J.V. Acrivos, Lei Chen and C.M. Burch, *Superlattices and Microstructures*, **18**, 197 (1995); (b) J.V. Acrivos, Lei Chen, P. Metcalf, J.M. Honig, R.S. Liu and K.K. Singh, *Phys. Rev. B*, **50**, 13710 (1994); (c) J.V. Acrivos, Lei Chen, C. Jiang, H. Nguyen, P. Metcalf and J.M. Honig, *J. Solid State Chem.* **111**, 343 (1994); (d) J.V. Acrivos, H.P. Hughes and S.S.P. Parkin, *J. Chem. Phys.* **86**, 1780 (1987); (e) J.V. Acrivos, *Mol. Cryst.*, **284**, 411 (1996)
4. L.D. Landau and E.M. Lifshitz, "*Statistical Physics*", translated by J.B. Sykes and M.J. Kearsley, Pergamon Press NY 1993
5. (a) P.G. de Gennes, *Phys Rev.* **118**, 141 (1960); (b) C. Castellani, C. Di Castro and M. Grilli, *Z. Phys. B* **103**, 137 (1997); (c) J. Tallon, personal communication.
6. (a) P.W. Atkins, "*Physical Chemistry*", 6th Edition, W.H. Freeman and Co, New York, 1998; J.V. Acrivos, K. Hathaway, J. Reynolds, J. Code, S. Parkin, M.P. Klein, A. Thompson and D. Goodin, *Rev. Sci. Instrum.* **53**, 575 (1982); (c) M. J. Latimer, A. Rompel, J. H. Underwood, V.K. Yachandra and M.P. Klein, *Rev. Sci. Instrum.* **66**, 1843 (1995); (d) A. Abragam and B. Bleaney, "*Electron Paramagnetic Resonance*", Oxford (1970)
7. C.T. Lin, W.Zhou and Y. W. Liang, *Physica C*, 195 291 (1992)

8. (a) X. Yao and J.M. Honig, *Mater. Res. Bull.* **29**, 709 (1994); (b) X. Yao et al., *Mater. Res. Soc. Proc.*, **453**, 291 (1997); (c) *Phys. Rev.* **B54** 17469 (1996); *ibid.*, **B56**, 7129 (1997)
9. (a) F.K. Richtmyer, S.W. Barnes and E. Ramberg, *Phys. Rev.* **46**, 843 (1934); (b) A.L. Ankudinov and J.J. Rehr, *J. Phys. IV France* **7**, C2-121 (1997); (c) A. Kodre, I. Arçon and R. Frahm, *ibid.*, C2-195 (1997); (d) Y.A. Babanov, A.V. Ryazhkin and A.F. Sidorenko, *ibid.*, C2-277 (1997); (e) G. Li, F. Bridges, G.S. Brown, *Phys. Rev. Lett* **68**, 1609 (1992); (f) C. Brouder, *J. Phys.:Condens. Matter* **2**, 701 (1990)
10. (a) R.S. Howland, T.H. Geballe, S.S. Laderman, A. Fischer-Colbrie, M. Scott, J.M. tarascon, P. Barboux, *Phys.Rtev.*, **B39**, 9017 (1989); (b) N. Watanabe and N. Koshizuka, *Advances in Superconductivity IX*, p. 153 , Springer-Verlag, Tokyo (1997); (c) C. Thomsen and M. Cardona, *Physical Properties of High Tc Superconductors I*, p. 409 (1988), World Scientific, D. M. Ginsberg, ed; (e) C. H. Booth, F. Bridges, J.M Boyce, T. Claeson, B.M. Lairson, R. Liang, and D. Bonn, *Phys. Rev.*, **B54**, 9542 (1996); (f) D.M. Ginsberg, *Physical Properties of High Tc Superconductors I*, p. 1 (1988), World Scientific, D. M. Ginsberg, ed; (g) D.M. Hazen, *Physical Properties of High Tc Superconductors II*, p. 121 (1989), World Scientific, D. M. Ginsberg, ed; (h) D.H. Templeton, *Handbook of Synchrotron Radiation*, **3**, 201 (1991), eds., G. Brown and D.E. Moncton, Elsevier; (i) M.a. Aranda, D.C. Sinclair, J.P. Attfield, A.P. MacKenzie, *Phys. Rev.*, **B51**, 12747 (1995); (j) J.V. Acrivos, to be published.
11. B.K. Teo, "EXAFS", Springer-Verlag, Berlin (1985)
12. J.V. Acrivos, S.S.P.Parkin, J.R.Reynolds, J.Code and E.Marseglia, *J.Phys. C.* **14**, L349 (1981)
13. S. Wolfram, "Mathematica", Cambridge University Press (1996)
14. (a)Y. DeWilde, N. Miyakawa, P. Guptasarma, M. Iavarone, L. Ozyuzer, F.J. Zasadzinski, P. Romano, D. G. Hinks, C. Kendziora, G. W. Crabtree And K.E. Gray, *Phys. Rev Lett.*, **80**, 153 (1998); (b) A. S. Alexandrov, *Physica C*, **305**, 46 (1998)

15. (a) H.S. Jarrett, R.J. Bouchard, J.L. Gillson, G.A. Jones, S.M. Marcus, and J. F. Weiher, *Mat. Res. Bull.*, **8**, 877 (1973); (b) R.J. Bouchard, J.L. Gillson and H.S. Jarrett, *ibid*, **8**, 489 (1973)

**Appendix I:** The relations used to interpret XAS of atom  $A$  in a solid material are<sup>a,b</sup>:

$$A_A(T) = K_A(m = 2\pi \tau/h, (E - E_0)) + \quad (I.1)$$

$$\sum_{AB} \sin\{\phi_{BA}(T) + 2 \mathbf{k} \cdot \mathbf{R}_{AB}(T)\} / (\mathbf{k} \cdot \mathbf{R}_{AB}(T))^2 S_A(\mathbf{k}) F_B(k, \pi) \exp(-2 k^2 \sigma_{AB}^2(T)) \exp(-2 R_{AB}/\lambda_{AB}(T)),$$

and,

$$K_A(\tau, E-E_0) = \int_0^{E-E_0} N(E_E) / [1 + (m x)^2]. \quad (I.2)$$

$k(\text{\AA}) = (0.2625(E - E_0))^{1/2}$  when  $E$  is in eV, the initial and final states energies are  $E_A$  and  $E_E$  respectively,  $\tau = 6.5821 * 10^{-16}$  s/(half width at half height in eV),  $E_{AE} = E_E - E_A = h\nu_{AE}$ ,  $x = E - E_{AE}$ ,  $m = 2\pi \tau/h$ , and the density of states  $N(E_E)$  is determined by the material. The first term is usually an order of magnitude greater than the second one.

---

<sup>a</sup> The second term in (I.1) represents the x-ray absorption fine structure (XAFS); it involves the sum over  $N_B$ ,  $B$  atoms (at  $R_{AB}$ ) which back scatter the photoelectron to  $A$  with strength  $S_A(k)$ ,  $F(k, \pi)$ ;  $\phi_{BA}(T)$ ,  $\sigma_{AB}$ , and  $\lambda_{AB}$  represent the combined phase shifts, the A-B bond Debye-Waller factor, and the mean free path of the photoelectron, respectively. A Fourier transform of this term gives the A-B bond distances versus  $T$ <sup>4-7,11,12</sup>.

<sup>b</sup> The shape of the atomic absorption coefficient  $K_A$  versus  $E - E_0$  is determined by the integral, evaluated numerically, using Mathematica<sup>13</sup> for a free electron gas density of states  $N(E_E) = C(E_F + x)^{0.5}$  where  $E_F = 10$  eV in Figures 4 to 6. Other DOS with a maximum near  $E_F$  in reference 14 have been tried. They all give rise to a positive slope  $dK/d(E-E_0)$  even when  $E_F$  changes by 37 meV<sup>14b</sup>. Also, though the Fermi energy may change at the transition, it is not expected to go back to the original value above  $T_c$ . Therefore, it is assumed that relaxation time changes are the dominant terms in  $K_A$ .

### List of Figures:

**Figure 1:** ESR of Superconducting Cuprates: **(a)** Dysonian shaped triplet state esr due to spin transitions  $\Delta S = 0$  in  $\text{YBa}_2\text{Cu}_3\text{O}_{7-\delta}$  single crystal near 5 K,  $c \parallel \mathbf{B}_z$ . The exact zero field,  $\mathbf{H} = 0$  is determined by the energy loss signal. Magnetic oscillations, due to flux motion, are observed above  $\mathbf{H} = 0$  in field cooled samples. No  $g = 2$  doublet esr is detected; triplet, T esr indicates  $\tau_T \approx 10^{-8}$  s and  $\tau_D \ll 10^{-10}$  s. **(b)**  $\text{Nd}(\text{Ba}_{0.95}\text{Nd}_{0.05})_2\text{Cu}_3\text{O}_7$  powder esr saturation experiment. Two types of centers are identified. c1 does not saturate at room temperature. c2 saturates easily and shows hfs due to  $^{143,145}\text{Nd}(I = 7/2)$ , 12.2 and 8.3 % respectively abundant with coupling constants:  $^{145}\text{A} = 4$  mT and  $^{143}\text{A} = 6.5$  mT in the ratio of the nuclear moments:  $^{143}\mu / ^{145}\mu = 1.59$ . Both c1 and c2 esr vanish above  $T_c$  (ref. 3a).

**Figure 2:** ESR of Organic Metal  $(\text{BEDT-TTF})_3\text{Ta}_2\text{F}_{11}$  (ref 3e): **(a)** Doublet (D) state esr at different T show transition from Lorentzian to Gaussian shape esr near 150 K, associated with the appearance of AF resonance. **(b)** AF resonance and triplet resonance absorption at different temperatures T.

**Figure 3:** XAS Configuration for the measurement in transmission at SSRL. The actual mounted crystal CT:  $\text{YBa}_2\text{Cu}_3\text{O}_{7-\delta}$  (Figures 4 to 6) is shown under the diagram.

**Figure 4:** Cu K-edge XAS of Single Crystal  $\text{YBa}_2\text{Cu}_3\text{O}_{7-d}$  (CT) as grown at the IRC for superconductivity, ref. 7). **(a)** XAS versus T. The constant sample density versus T is ascertained by  $A_{y,max} = 1.8 \ln(10)$  versus T. **(b)**  $A_{\text{Cu}}(60 \text{ K}) - A_{\text{Cu}}(T \neq T_c)$ . **(c)**  $A_{\text{Cu}}(92 \text{ K}) - A_{\text{Cu}}(T \neq T_c)$ . **(d)**  $\mu_{\text{Cu}}$  versus  $\varphi$  (Figure 3). The spectrometer stability is confirmed by the Cu foil reference stability. **(e)**  $\mu_{\text{CuE}}$  vs  $\theta$ . The insert  $\mu_{\text{CuEn}} = \mu_{\text{CuE}} / \cos(\theta - \pi/2)$  confirms the dipolar symmetry.  $\mu_{\text{CuEpz}} = [\mu_{\text{CuEn}}(\pi/4) - \mu_{\text{CuE}}(\pi/2)] / \sin(\pi/4)$  obtains the z contribution  $p_0$  with a line width of the order of 3 eV. **(f)** Calculated  $\mu_{\text{CuEn}}$ , for  $E_0\text{Cu}(\text{chains}) - E_0\text{Cu}(\text{planes}) = 6$  eV compared to T averaged data.

**Figure 5:** Ba L<sub>3,2</sub>-edge XAS of CT, YBa<sub>2</sub>Cu<sub>3</sub>O<sub>7-d</sub> single crystal and 2 $\mu$ m powder Nd(Ba<sub>0.95</sub>Nd<sub>0.05</sub>)<sub>2</sub>Cu<sub>3</sub>O<sub>7</sub>, 1:5 weight ratio in BN. **(a)** CT L<sub>3</sub> edge intensity stability from  $\theta = \pi/2$  to  $8\pi/18$  as T decreases below T<sub>c</sub>. **(b)** L<sub>3,2</sub> XAFS enhancement versus T at  $\theta = 8\pi/18$ . **(c)** XTDAS relative to T<sub>max</sub> at  $\theta = 8\pi/18$ . **(d),(e)** A<sub>Ba</sub>(L<sub>3</sub>), A<sub>Ba</sub>(L<sub>2</sub>) enhancement showing interference pattern at  $\theta = 8\pi/18$ . **(f)** k<sup>3</sup>XTDAS at two T intervals showing change in AT-XAFS near T<sub>c</sub> ~ 60 K. **(g)** XTDAS relative to T<sub>c</sub> for spectra Ba-L<sub>3</sub> XAS versus T for 2 $\mu$ m powder Nd(Ba<sub>0.95</sub>Nd<sub>0.05</sub>)<sub>2</sub>Cu<sub>3</sub>O<sub>7</sub>.

**Figure 6:** Y K-edge XAS in CT, YBa<sub>2</sub>Cu<sub>3</sub>O<sub>7-d</sub>: **(a)**  $\mu_{YE}(\theta)$  versus  $\theta$ , with orientation dependence similar to  $\mu_{CuE}$ . **(b)**  $\mu_{YE}(\pi/4) - \mu_{YE}(\theta = n\pi)$  at 65 K. When  $\theta = 17\pi/36$ , the interference fine structure is  $dE_Y = 1.27 \text{ eV} \sim 2 dE_{Ba}$ . Here  $\lambda = \lambda_{Ba \text{ L-edge}}/3 \text{ \AA}$  indicates that third order diffractions of those near the Ba edge may be responsible for the energy shifts (by diffraction) that cause the interference pattern. The absorbers involved, may be those occurring as impurities in the Ba layer. **(c), (d), (e)** Change in Y AT-XAFS vs T at different  $\theta$  below T<sub>c</sub> = 92 K.

**Figure 7:** XTdAS for 2  $\mu$ m size powder NiS<sub>2-x</sub>Se<sub>x</sub> (x = 0.47: m<sub>3</sub> cubic lattice a = b = c = 5.753(9)  $\text{\AA}$  in ref. 2b) diluted in 1 to 5 parts per weight in BN near the Se-K edge. The spectrometer stability is confirmed by the Se film reference XAS, and the constant sample density by the constant edge  $A_v = 0.125 \text{ Ln}(10)$  versus temperature for all the spectra.

**Figure 8:** Lower limit of the state uncertainty in entropy,  $\Delta S/k_B$ , for the doublet D, triplet T and antiferromagnetic, AF states in the organic metal BEDTTF)<sub>3</sub>Ta<sub>2</sub>F<sub>11</sub> as it approaches the transition to superconductivity near 10 K.

**Figure 9:** La<sub>2</sub>NiO<sub>4.00</sub>: Lower limit of the state uncertainty in entropy  $\Delta S/k_B \geq h/(4 k_B \pi \tau T)$  from magnetic resonance relaxation times  $\tau$  versus absolute temperature T (ref. 3c).

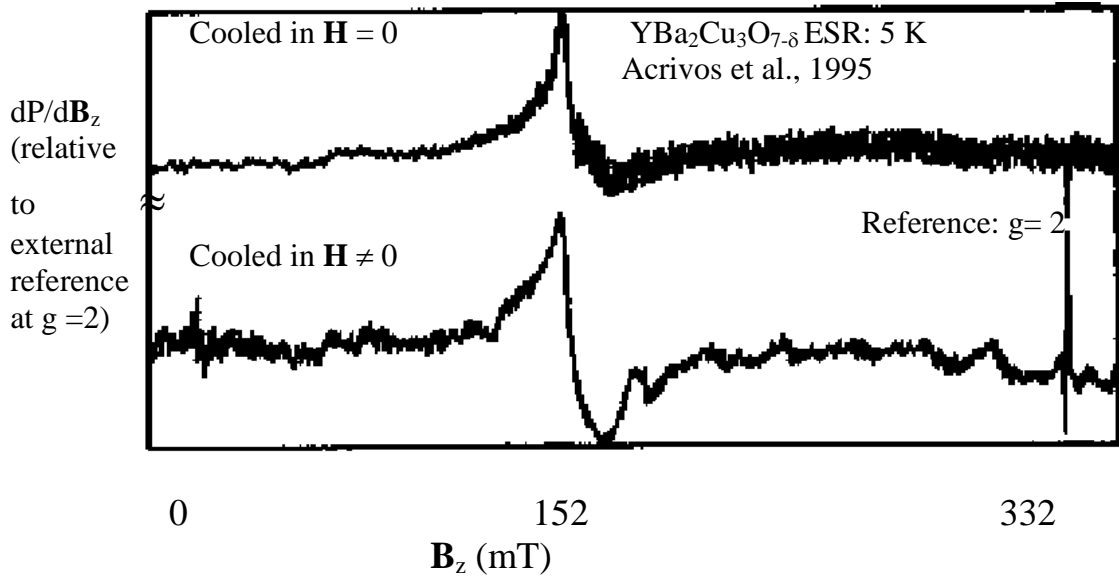


Figure 1a

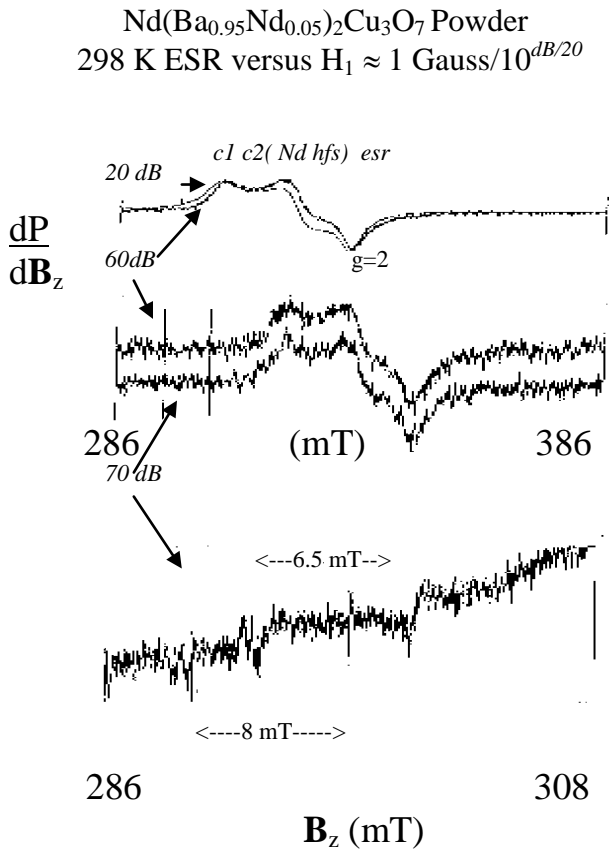
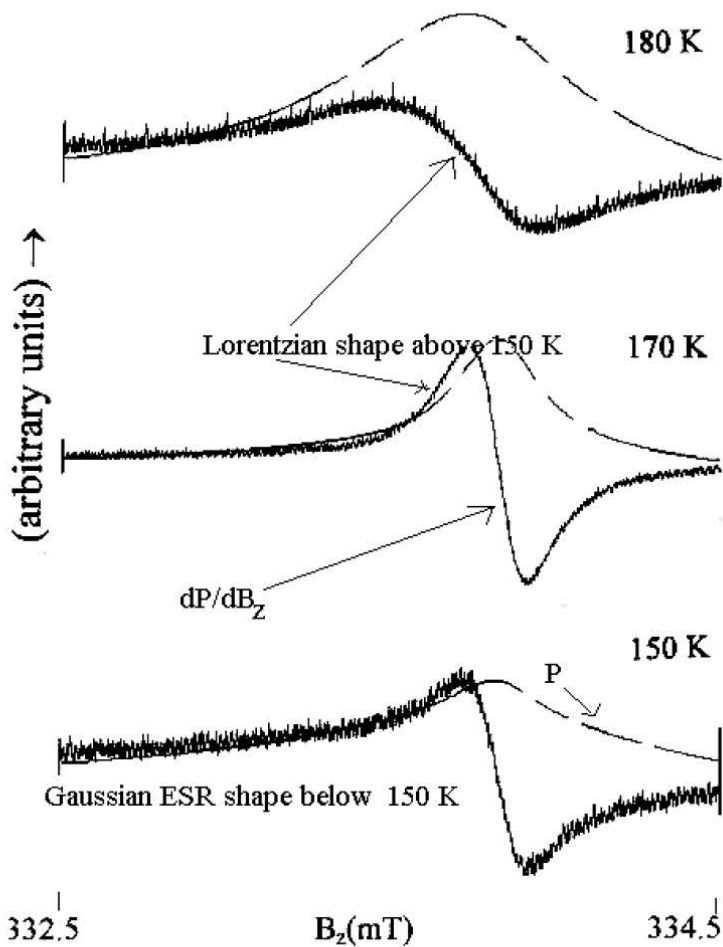


Figure 1b



$(\text{BEDT-TTF})_3\text{Ta}_2\text{F}_{11}$ ,  $\theta=70^\circ$ , (20 dB)

D, ESR above and below  $T_{00} = 150$  K



$(\text{BEDT-TTF})_3\text{Ta}_2\text{F}_{11}$ ,  $\theta=0^\circ$

Antiferromagnetic (AF) and Triplet ( $T^*$ ) ESR above  $T_c$

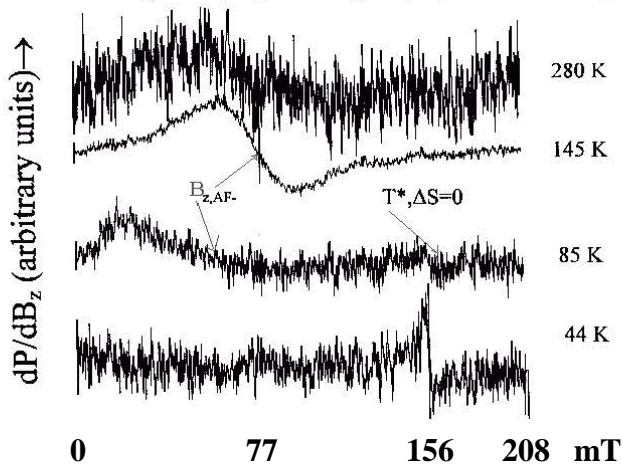
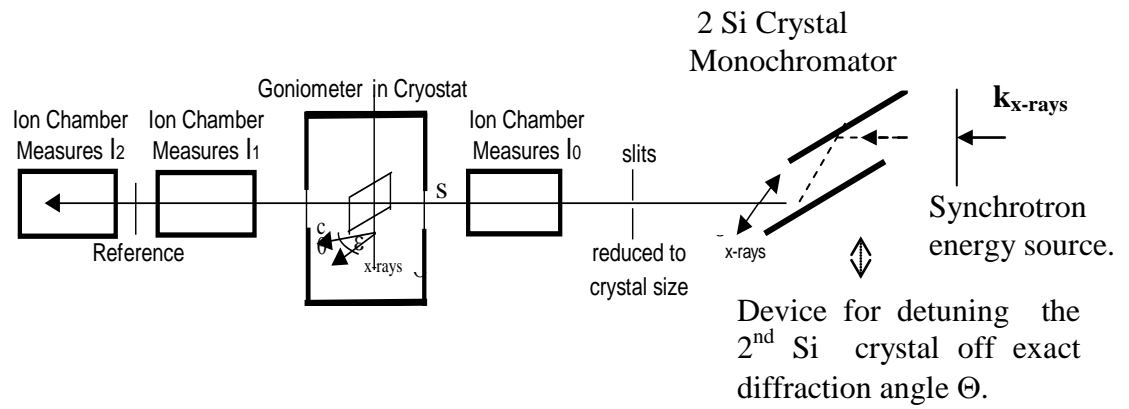
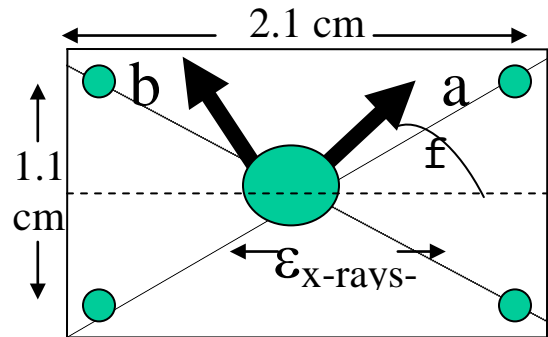


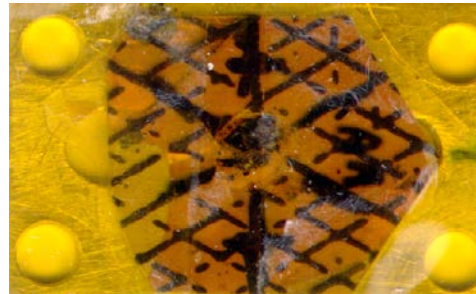
Figure 2: (a) (b)



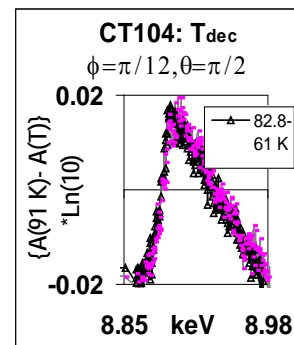
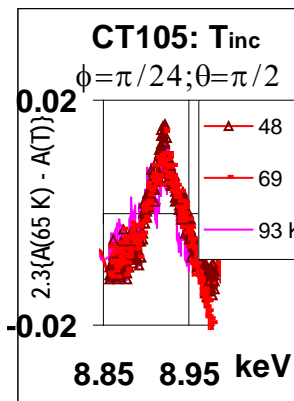
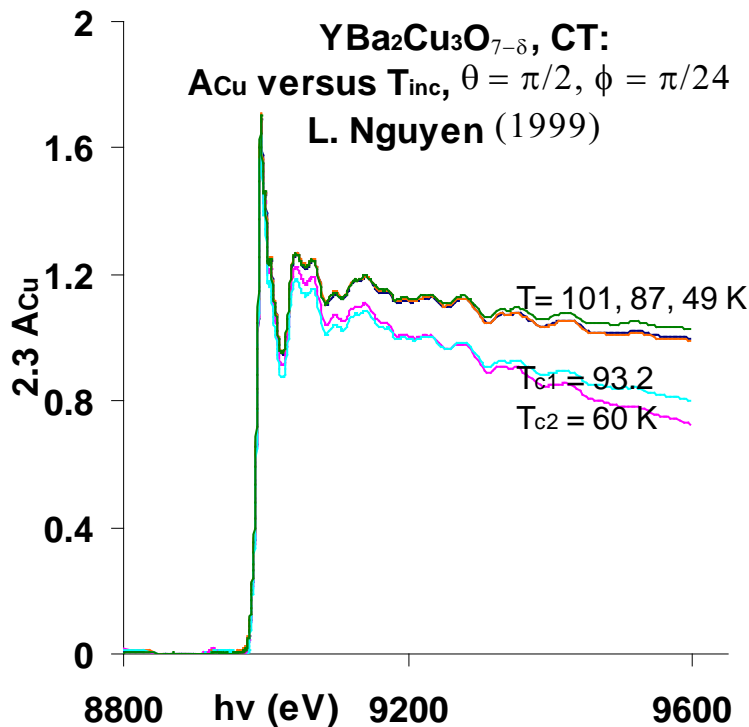
Sketch of sample mount inside the above Oxford Cryostat:  $\theta = \mathbf{c} \wedge \boldsymbol{\varepsilon}_{\text{x-rays}}$  is determined outside the cryostat by a goniometer to  $\pm 2$  DEG.

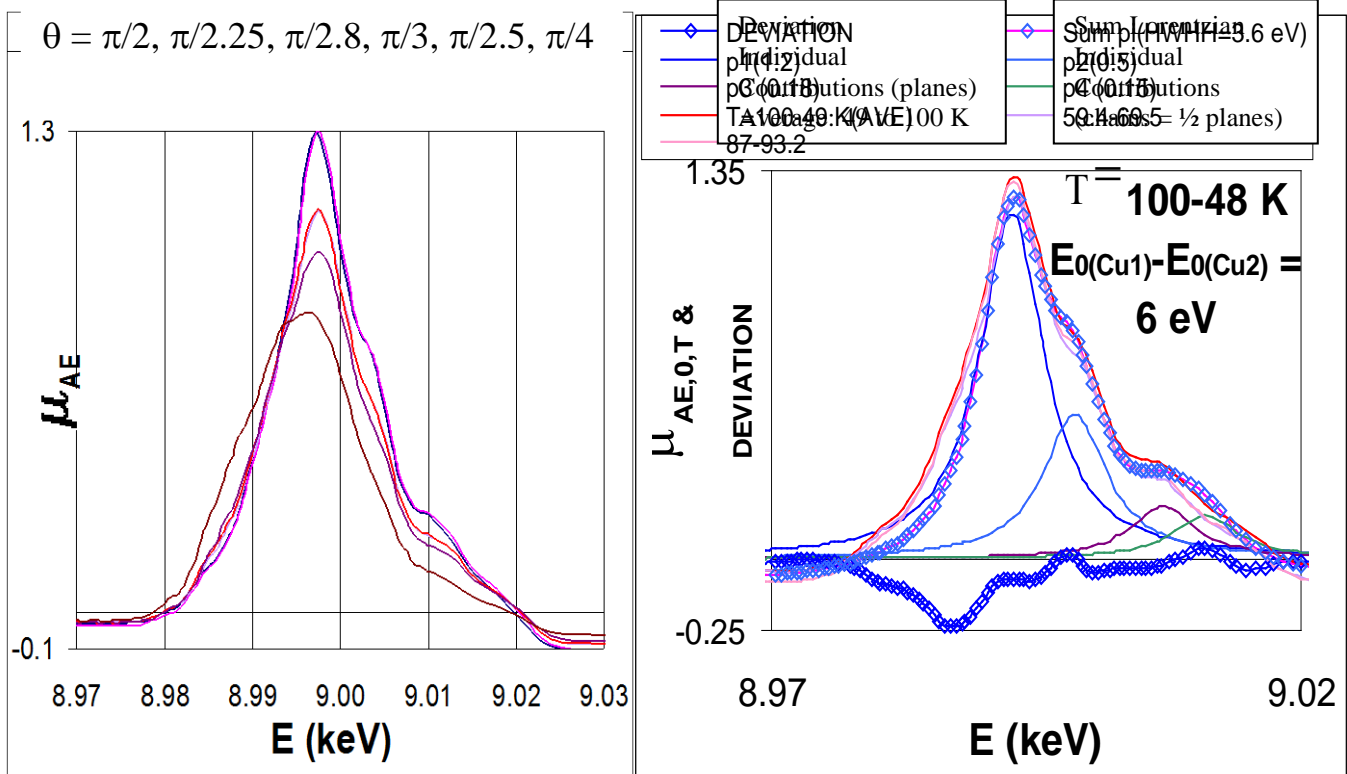
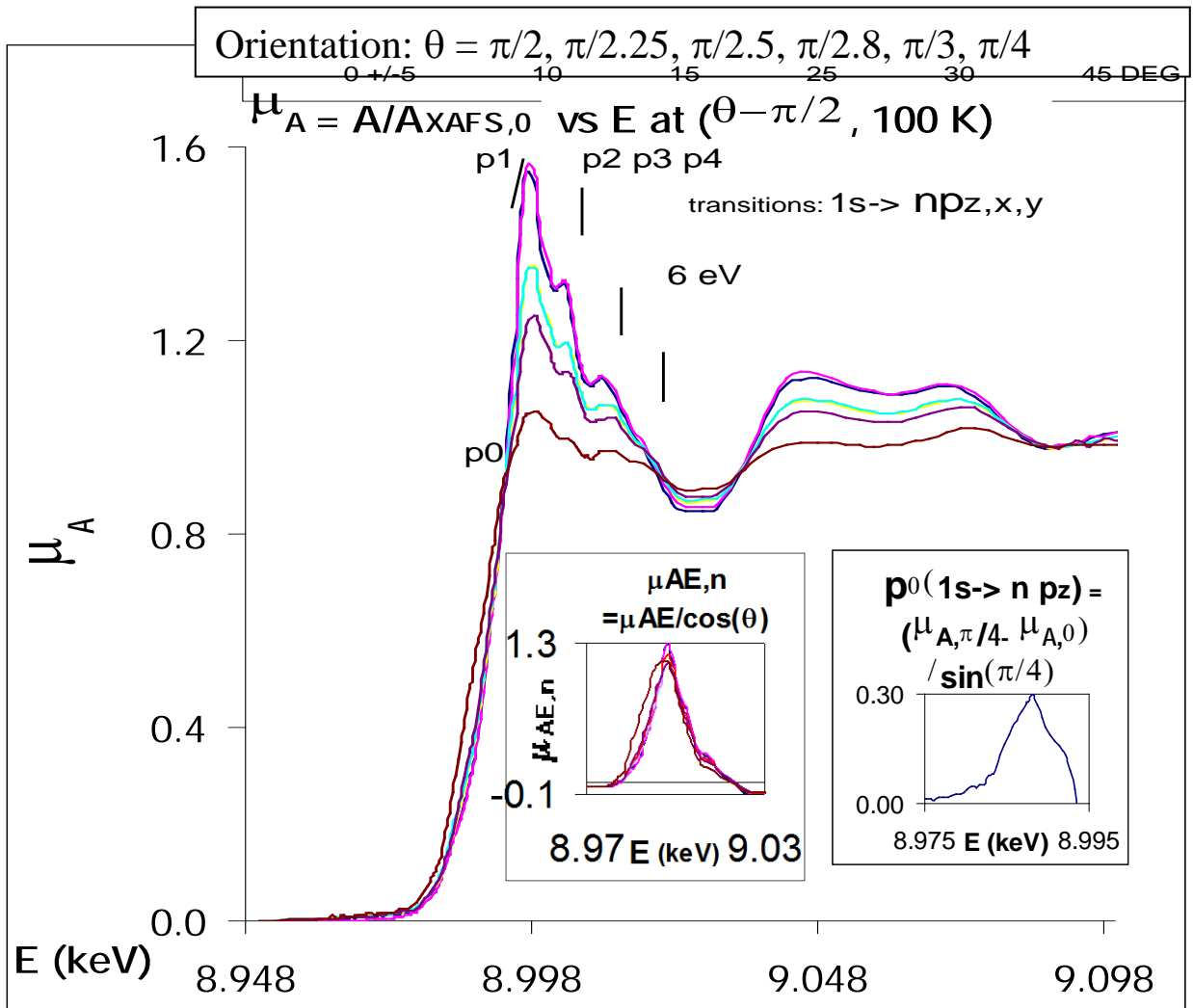


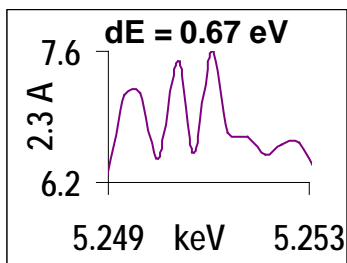
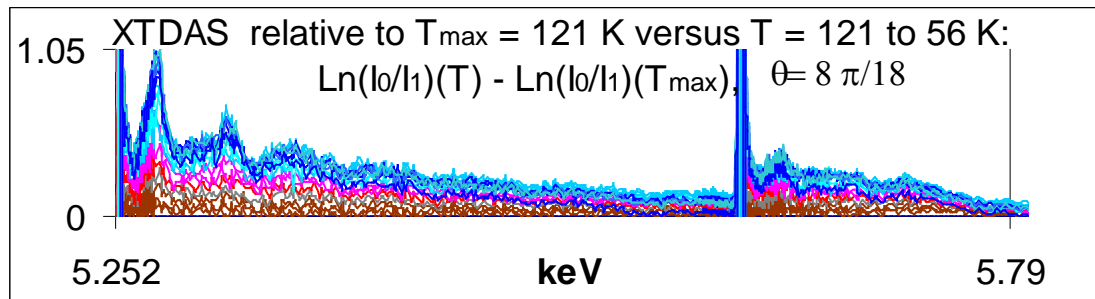
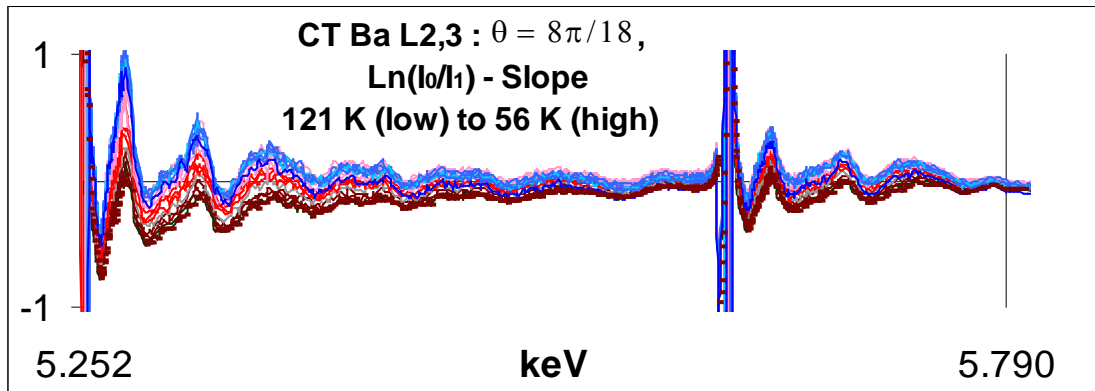
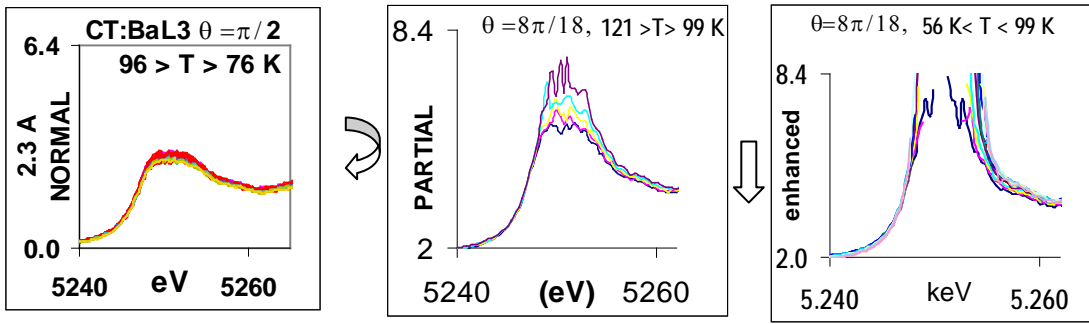
CT crystal as mounted, with a lead mask and a grid to determine the orientation  $\phi$ , is also shown.



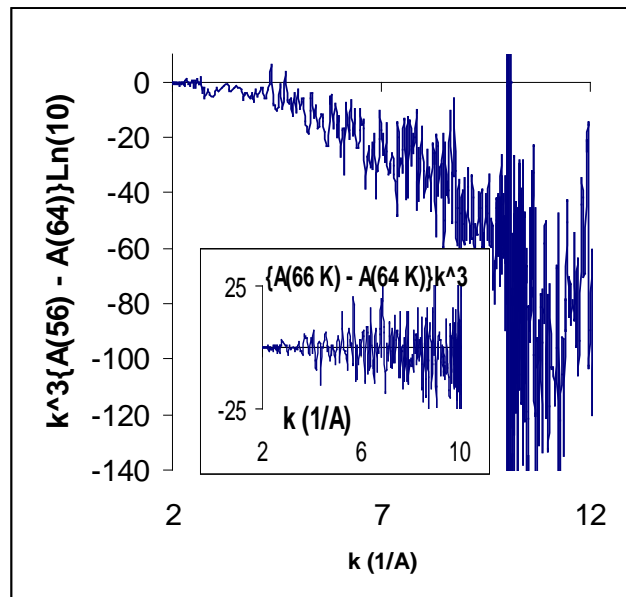
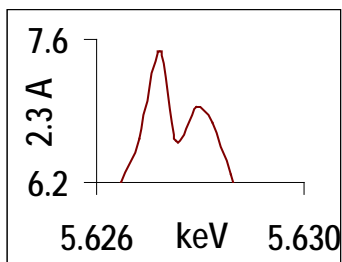
Figures 3  $\uparrow$  and 4a to f  $\downarrow$



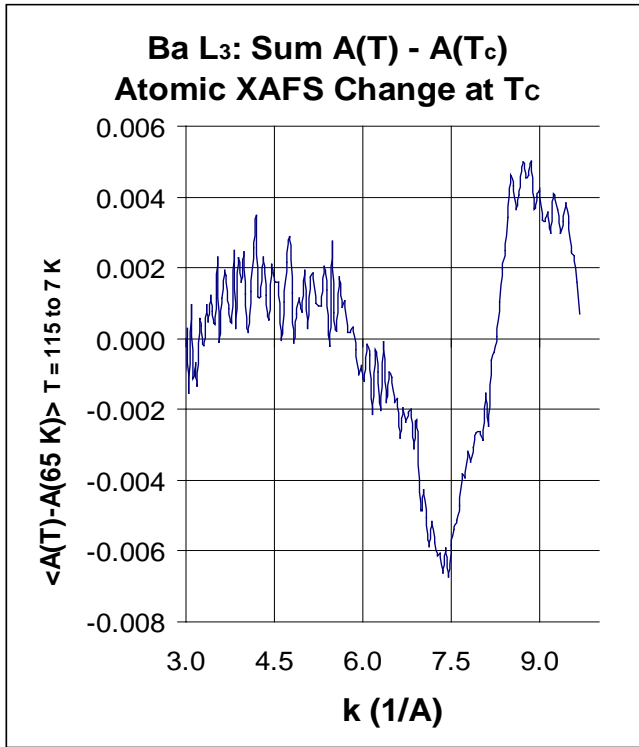




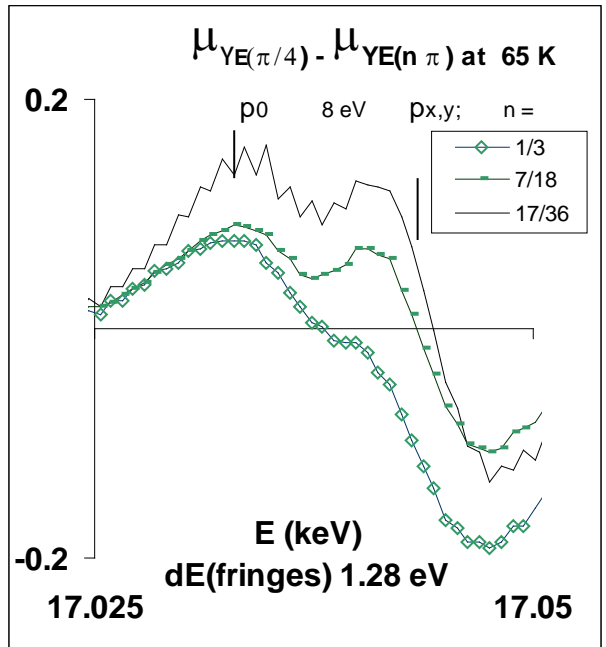
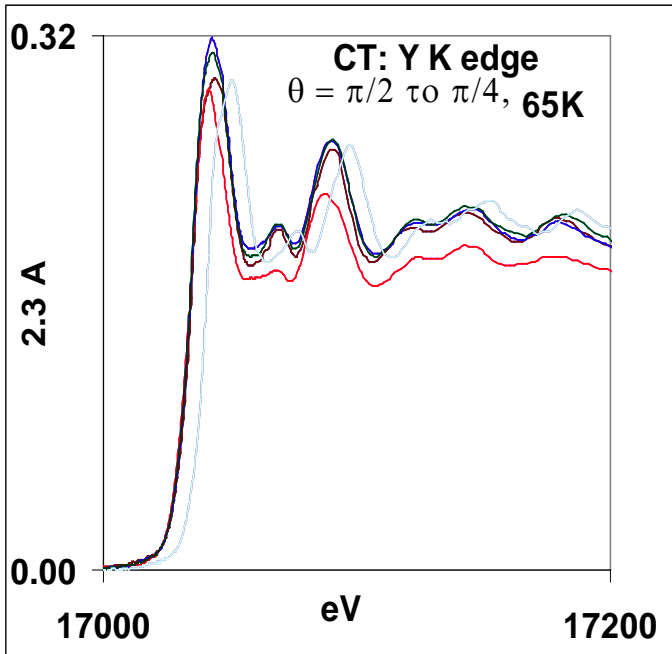
L3,2 Edge Fringes, 99 ± 2K

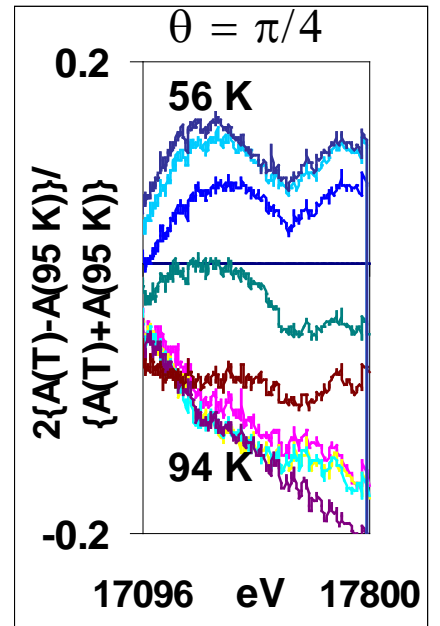
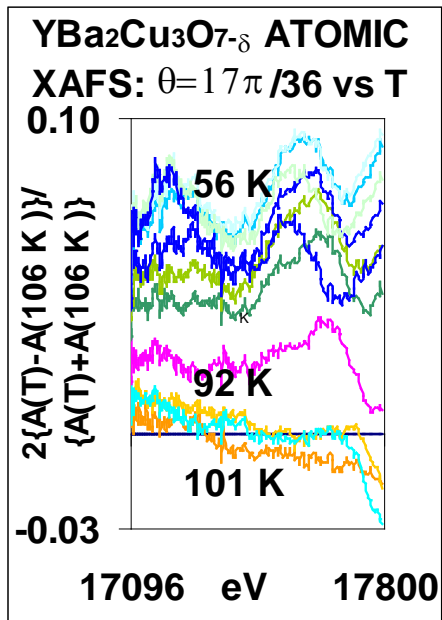
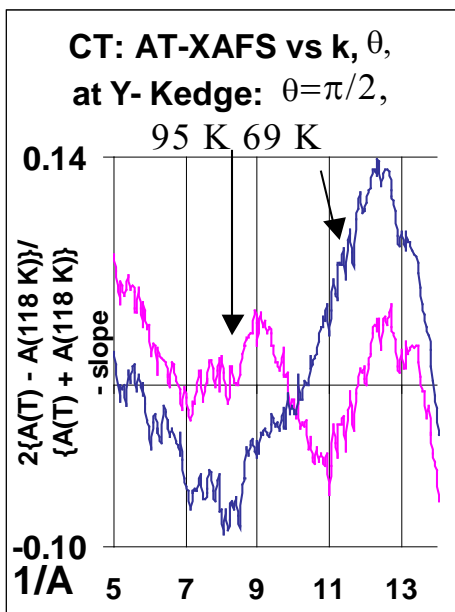


Nd(Ba<sub>0.95</sub>Nd<sub>0.05</sub>)<sub>2</sub>Cu<sub>3</sub>O<sub>7</sub> (1:5 in BN) Ba-L3 edge



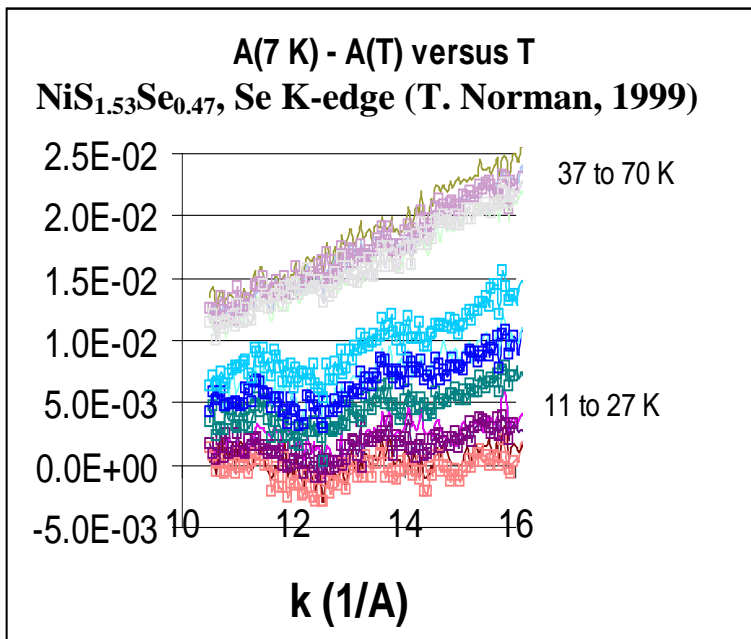
Figures 4 a to g ↑





Figures 6a to e  $\uparrow$

Figure 7  $\downarrow$



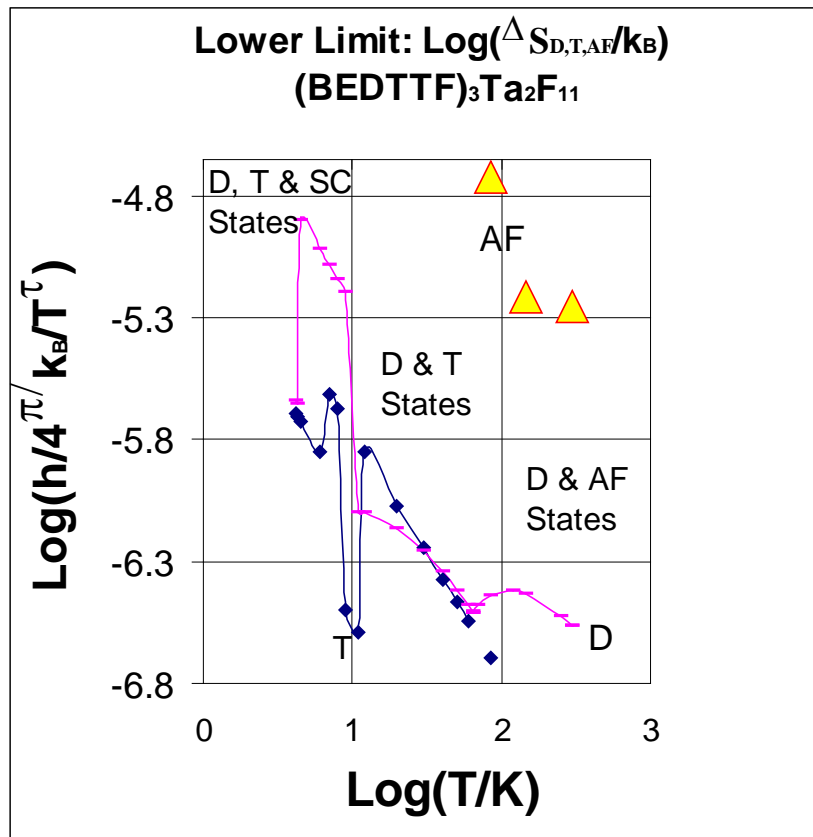


Figure 8

Figure 9

